Tristan Aillet, Karine Loubiere*, Odile Dechy-Cabaret, and Laurent Prat

Accurate Measurement of the Photon Flux Received Inside Two Continuous Flow Microphotoreactors by Actinometry

Abstract: In this study, the photon flux received in two continuous flow microphotoreactors was measured by actinometry (potassium ferrioxalate). The microphotoreactors had two different geometries and were irradiated by either a polychromatic or a monochromatic light source. A model considering the partial absorption of photons through the reactor depth and, if required, the polychromatic character of the light source and the dependence of the actinometer properties on the wavelength were formulated to describe the variation of the actinometer conversion with the irradiation time. The photon flux received in the microphotoreactors could be thus accurately calculated as a function of the emitted wavelength. The same methodology was then applied to measure the photon flux received in a batch immersion well photoreactor. The radiant power received in each photoreactor was compared to that emitted by the lamp and major differences were found, thus confirming the need for this kind of in situ measurement. Finally, some guidelines based on a knowledge of the photon flux were proposed to compare various photoreactors. They revealed in particular that the choice of the most efficient photoreactor depended on the criteria chosen to evaluate the performances (i.e. productivity, Space Time Yield).

Keywords: photochemistry, microphotoreactor, chemical actinometry, photon flux

***Corresponding author: Karine Loubiere,** Université de Toulouse, INPT, ENSIACET, F-31432 Toulouse, France; CNRS, Laboratoire de Génie Chimique (LGC UMR 5503), 4 allée Emile Monso, BP 84234, F-31432 Toulouse, France, E-mail: karine.loubiere@ensiacet.fr
Tristan Aillet, Université de Toulouse, INPT, ENSIACET, F-31432 Toulouse, France; CNRS, Laboratoire de Génie Chimique (LGC UMR 5503), 4 allée Emile Monso, BP 84234, F-31432 Toulouse, France, E-mail: tristan.aillet@ensiacet.fr
Odile Dechy-Cabaret, Université de Toulouse, INPT, ENSIACET, F-31432 Toulouse, France; CNRS, Laboratoire de Chimie de Coordination (LCC UPR 8241), 205 route de Narbonne, BP 44099, F-31077 Toulouse, France, E-mail: odile.dechycabaret@ensiacet.fr
Laurent Prat, Université de Toulouse, INPT, ENSIACET, F-31432 Toulouse, France; CNRS, Laboratoire de Génie Chimique (LGC UMR 5503), 4 allée Emile Monso, BP 84234, F-31432 Toulouse, France, E-mail: laurent.prat@ensiacet.fr

1 Introduction

Recently, microreactor technology has been successfully investigated in the organic chemistry field. The micro-scale offers several advantages, such as short molecular diffusion distances, intensified heat and mass transfers, and small amounts of reactants used. In the case of photochemistry, microreactors also allow efficient light penetration even for relatively concentrated solutions. For these reasons, microreactors are increasingly being adopted for photochemical reactions, including photocycloadditions, photooxygenations, photoisomerizations and photocatalytic reactions (Coyle and Oelgemöller 2008; Oelgemoeller 2012; Knowles, Elliott, and Booker-Milburn 2012). Although the benefits of microreactors for photoconversion are now accepted, there is still a lack of objective criteria for understanding and modelling the positive effect of the microspace, and thus for rigorously transposing photochemical synthesis from batch to intensified continuous flow reactors. This requires a modelling approach in which hydrodynamic and radiative transfer phenomena are coupled via the reaction kinetics term. In addition, microreactors are widely used for studying reactions and acquiring the associated kinetic data (Mozharov et al. 2011). By analogy, we could imagine using microreactors to determine some intrinsic properties of a photochemical reaction, such as the quantum yield.

In all cases, for modelling, for data acquisition purposes, or for optimizing reaction performance, it is essential to know the photon flux (einstein s^{-1}) actually received in the continuous flow microphotoreactor. Up to now, this photon flux has not been accurately measured in such systems, and most studies have estimated this parameter either by a modelling approach (Aillet et al. 2013) or from the characteristics of the light source (Sugimoto et al. 2009; Shvydkiv et al. 2011; Aida et al. 2012). For example, Sugimoto et al. (2009) carried out the Barton reaction of a steroidal substrate in various continuous microphotoreactors and compared the reaction performances according to the light sources and the material of the microreactor glass top. To do this, they measured the characteristics of the light transmitted through each type of reactor top. Shvydkiv et al. (2011) compared the

performances of a batch Rayonet reactor and various microreactors. They used the data given by the lamp manufacturer and evaluated, for example, the lamp power per unit of irradiated surface (W cm^{-2}). In a recent paper (Aillet et al. 2013), we deduced the photon flux from a modelling approach in which the polychromatic light source was assumed to be monochromatic, and hence pointed out the important role of the photon flux when comparing different photoreactors. Thus, in all cases, the photon fluxes considered remain approximate in so far as they are not equal to the fluxes actually received in the microphotoreactor, which depend, of course, not only on the characteristics of the light source but also on the reactor exposition to the source, on the reflectance and transmittance of the reactor material.

In classical photoreactors, the photon flux is commonly determined by direct measurements using a radiometer. However, this method cannot be applied in microreactors since their dimensions are smaller than those of the sensor and also because, in most cases, the irradiated area remains difficult to determine accurately. An efficient alternative is to use an actinometer, which involves a simple photochemical reaction with a known quantum yield. Despite that this well-established method is commonly applied in photochemical reactors of large scale (see for example (Yang, Pehkonen, and Ray 2004; Yang et al. 2005; Cornet, Marty, and Gros 1997; Zalazar et al. 2005)), we have not found any works implementing actinometry in microphotoreactors.

In this context, this article aims to show that the photon flux actually received in a continuous flow microphotoreactor can be accurately and easily measured by actinometry. The actinometer chosen was potassium ferrioxalate, as it is a standard one recommended by IUPAC (Kuhn, Braslavsky, and Schmidt 2004; Parker 1953; Hatchard and Parker 1956; Lehóczki, Józsa, and Ősz 2013; Allmand and Young 1931; Hook et al. 2005). The photon flux was measured in two continuous flow microphotoreactors of different geometries and irradiated by either a polychromatic light source (high-pressure mercury lamp) or a monochromatic light source (UV-LED array). Due to the reactor dimensions, some precautions were required to correctly transpose this standard method from the macro- to the micro-scale. Firstly, because part of the incident photon flux was inevitably transmitted over the reactor thickness, a kinetic model was necessary to account for this partial absorption of photons. In addition, as the measurements were, in some cases, performed under polychromatic irradiation without light filtering, the dependence of the intrinsic actinometer properties (quantum yield, Napierian molar absorption coefficient) on the wavelength was considered. Through this consistent analysis, it was possible to model the experimental variation of the actinometer conversion with the irradiation time and thus to accurately calculate the photon flux received in the microphotoreactor as a function of the wavelength emitted by the lamp. The same methodology was then used to measure the photon flux received in a batch immersion well photoreactor. Finally, the radiant power received in each photoreactor was compared to that emitted by the lamp, and some guidelines based on a knowledge of the photon flux were proposed to compare various photoreactors.

2 Material and methods

2.1 Microphotoreactors and batch photoreactor

The first continuous flow microphotoreactor (A) used in this study (Figure 1a) had a design encountered in many different studies (Aillet et al. 2013; Hook et al. 2005; Lainchbury et al. 2008; Vaske et al. 2010), classically named "capillary tower". It was constructed by winding Fluorinated Ethylene Propylene (FEP) tubing (508 μm inner diameter d, 1587.5 μm outer diameter, 4 m length) in a single pass around an immersion well made of Pyrex, which contained a high-pressure Hg lamp. The temperature was not measured directly inside the microphotoreactor, only the stability of the temperature (8°C) of the cooling water circulating in the double jacket was checked. Aluminium foil was also used to protect the supply syringe and the inlet and outlet sections of the tubing from UV light, thus ensuring that the photochemical reaction took place only in the tubing section wound around the well. The solution to be irradiated was fed into the reactor tubing by a high-pressure syringe pump (neMESYS High-Pressure Module, Cetoni®) equipped with 20 mL syringes.

The second continuous flow microphotoreactor (B) consisted of an FEP tube (508 μm inner diameter d, 1587.5 μm outer diameter, 2.65 m length) which was fixed in a channel carved in a flat aluminium plate (Figure 1b). To maximize the space, in particular with respect to the surface irradiated by the light source, the FEP tube was wound in a spiral geometry; the inlet of the tube was located at the centre of the spiral. The surface was then illuminated with a UV-LED array composed of 9 LEDS emitting at 365 nm. The radiant lamp power could be changed by varying the electrical intensity I_a supplying the UV-LED array. The height h between the UV-LED source and the irradiated surface (i.e. the FEP tube) was fixed at 10 cm in order to obtain uniform illumination at the reactor surface.

Some actinometry measurements were also run in a conventional batch photoreactor (Figure 1c) having the

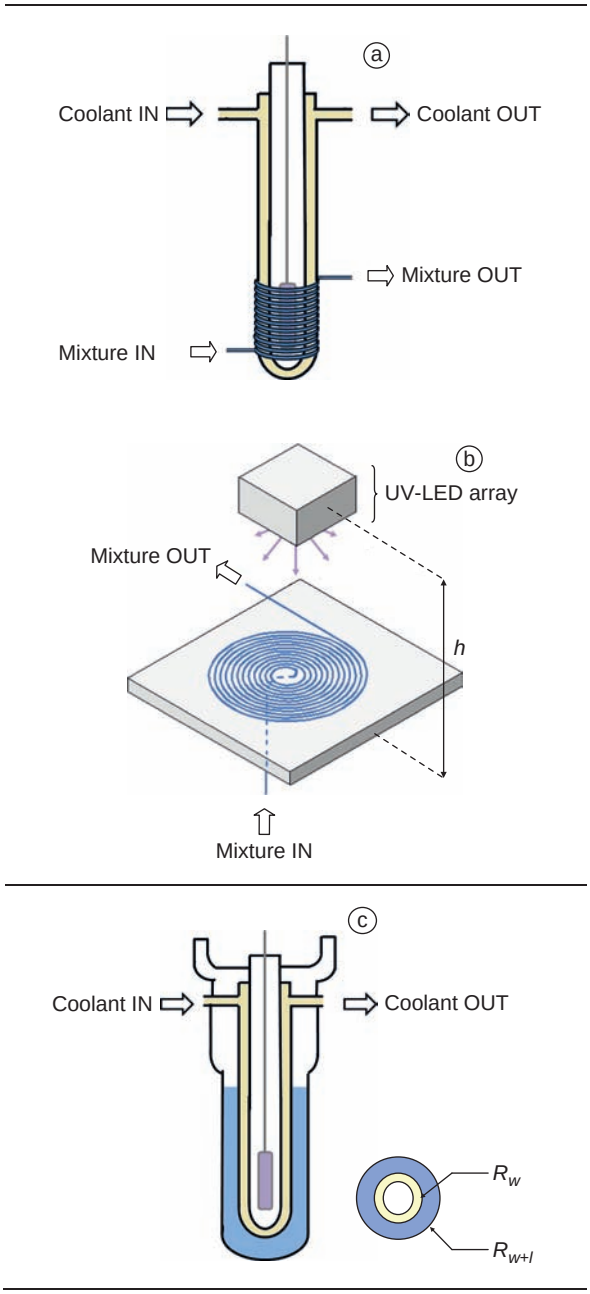

Figure 1 (a) Microphotoreactor A. (b) Microphotoreactor B. (c) Batch immersion well photoreactor

same immersion well and the same light source as the ones used for the microphotoreactor A. The volume of the irradiated solution, V_r, was equal to 225 mL here.

The main geometrical characteristics of the photoreactors are detailed in Table 1.

For the two photoreactors irradiated by the mercury lamp, radiations at wavelength below 300 nm were assumed to be completely absorbed by the Pyrex material leading to:

Table 1 Geometrical characteristics of the photoreactors

Parameters	Microphotoreactor		Batch photoreactor
	A	B	
Volume of reactor V_r (mL)	0.81	0.54	225
Optical path length l (cm)	0.0508	0.0508	0.62
Length of tube L (m)	4	2.65	–
Inner radius R_W (cm)	–	–	2.50
Outer radius R_{W+l} (cm)	–	–	3.12
Lamp type	High-pressure Hg lamp (Polychromatic)	UV-LED array (quasi-monochromatic)	High-pressure Hg lamp (Polychromatic)
Operating mode	Continuous	Continuous	Batch

$$T_{\lambda \leq 300} = 0, T_{\lambda > 300} = 1 \quad (1)$$

where T_λ is the material transmittance at the wavelength λ ($0 \leq T_\lambda \leq 1$). Note that, rigorously speaking, the complete transmittance spectrum of the Pyrex material should be considered. Nevertheless, as the radiant energy emitted by the mercury lamp near 300 nm is weak in comparison to the other radiations participating in the actinometry reaction, this assumption remains reasonable.

In the same way, the tubing material (i.e. FEP) was assumed to be completely transparent to UV radiation above 230 nm (Aida et al. 2012; Allmand and Young 1931).

2.2 Light sources

Two different light sources were used in this study.

The lamp used in the microphotoreactor A and in the batch photoreactor was a mercury vapour discharge lamp (high-pressure Hg Ba/Sr lamp, 125 W, HPK Heraeus®). According to its spectral distribution, the polychromatic behaviour of the lamp must be taken into account as no specific equipment for light filtering was used in the present experiments. Generally, manufacturers give the spectral distribution in terms of relative radiant exitance:

$$S_{e,\lambda} = \frac{M_{e,\lambda}}{M_{e,max}} \quad (2)$$

where the radiant exitance $M_{e,\lambda}$ represents the power emitted from the lamp per unit of source surface area (in W m^{-2}) at a given wavelength λ. $M_{e,\max}$ is the maximum value observed within the spectral emission domain of the lamp. Note that the subscripts "e" and

"p" denote the physical quantities expressed in radiometric units (i.e. in watts) and in photon units (i.e. in einstein s^{-1}) respectively.

Multiplying eq. (2) by $M_{e,\max}$ gives the radiant exitance of the lamp:

$$M_{e,\lambda} = M_{e,max} S_{e,\lambda} \tag{3}$$

Then, we convert this value into photon quantities, i.e. einstein s^{-1}.

$$M_{p,\lambda} = M_{e,max} S_{e,\lambda} \frac{1}{N_A \, \Delta E_\lambda} \tag{4}$$

where $\Delta E_\lambda = \frac{hc}{\lambda}$ is the energy of a photon (J), h the Planck constant (6.6256×10^{-34} J s), c the speed of light (2.9979×10^{8} m s^{-1}), and N_A the Avogadro constant (6.02×10^{23} mol^{-1}).

Lastly, the density function of the lamp, g_λ, is expressed for each wavelength as:

$$g_\lambda = \frac{M_{p,\lambda}}{\sum_{\lambda_i} M_{p,\lambda_i}} = \frac{\lambda \, S_{e,\lambda}}{\sum_{\lambda_i} \lambda_i \, S_{e,\lambda_i}} \tag{5}$$

where $\sum_{\lambda i} M_{p,\lambda_i}$ represents the summation of the power emitted at each wavelength. The values of the density function for the mercury lamp are presented in Figure 2: they confirm that, for the mercury lamp, the most important lines are at 365 nm, 436 nm and 546 nm.

The second light source used (microphotoreactor B) was a UV-LED array made by the company Led Engineering Development (Toulouse, France). It was built with 9 Nichia LED (models NCSU033B). The total output power was 2.925 W (325 mW per LED). According to the spectral distribution (Figure 2), the UV-LED source can be considered as monochromatic since the output energy is narrowly (± 10 nm) distributed around the 365 nm wavelength.

2.3 Actinometer

$$2\left[\mathrm{Fe}(\mathrm{C_2O_4})_3\right]^{3-} \rightarrow 2\mathrm{Fe}(\mathrm{C_2O_4}) + 3\left[\mathrm{C_2O_4}\right]^{2-} + 2\mathrm{CO_2} \tag{6}$$

The actinometer used in this study was potassium ferrioxalate. It is based on the photodecomposition of the complex $[Fe(C_2O_4)_3]^{3-}$ in water (eq. (6)). This actinometer is largely described in the literature (Kuhn, Braslavsky, and Schmidt 2004; Parker 1953; Hatchard and Parker 1956; Lehóczki, Józsa, and Ősz 2013; Allmand and Young 1931). It absorbs in a broad spectral domain and the quantum yield is relatively constant in this domain (300–450 nm). Moreover, the quantum yield does not depend on the temperature, the presence of oxygen in the mixture or reactant concentration (Parker 1953). Despite these well-established properties, the ferrioxalate actinometer suffers from its low solubility in water and from the precipitation of the ferrous oxalate produced when it is exposed to radiation. These characteristics were particularly disadvantageous when operating in a microphotoreactor: it was impossible to work under full absorption conditions. In addition, the precipitation of the ferrous oxalate made quantitative energy measurements difficult and, in the extreme, could lead to clogging of the microphotoreactor. Lastly, some gaseous carbon dioxide could be produced, thus generating bubbles in the microphotoreactor.

Consequently, to avoid significant gas generation, maintain a homogeneous solution and prevent clogging,

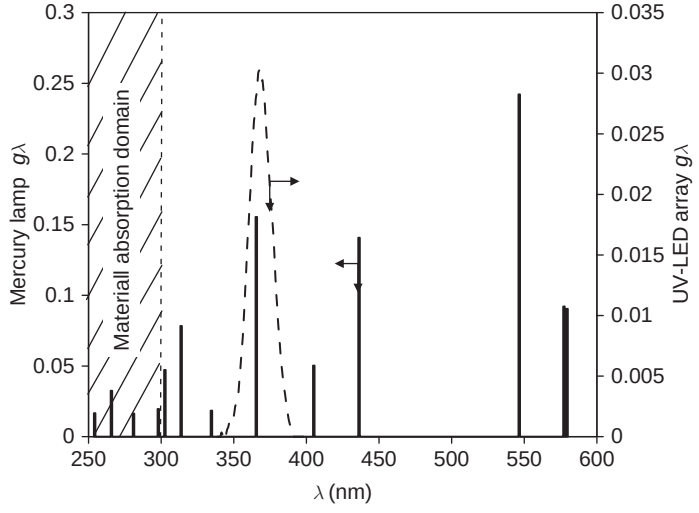

Figure 2 Density function g_λ of the lamps. Black bars correspond to the lines of the mercury lamp and dashed line corresponds to the spectral distribution of the UV-LED array

it was imperative to operate at low conversions. In practice, this implied working with short residence times (few seconds) and thus with high flow rates Q (see Table 3). For that, specific pumps and a high-pressure syringe (neMESYS High-Pressure Module, Cetoni®) were used to overcome large pressure drops (15–30 bars). Note that the range of the flow rates involved in the microphotoreactors A and B was not the same; this was due to the fact that the residence times required for keeping the conversions low were directly correlated to the radiant power of the lamps, which was significantly different in the two microphotoreactors (see Section 5.1).

Table 2 reports the set of experimental conditions for all the photoreactors. All the experiments were performed at an initial concentration C_{A0} of 0.16 mol L^{-1}, which corresponded to the maximum actinometer solubility observed. The conversions were always kept below 20%.

Table 2 Operating conditions for implementing actinometry in the two microphotoreactors and in the batch photoreactor (C_{A0} is the initial concentration of the ferrioxalate solution, X the actinometer conversion, τ the residence time in the microphotoreactor, t the irradiation time in the batch photoreactor)

Parameters	Microphotoreactor		Batch photoreactor
	A	B	
C_{A0} (mol L^{-1})	0.16	0.16	0.16
$C_{H_2SO_4}$ (mol L^{-1})	0.2	0.1	0.1
X (%)	$10 < X < 20$	<10	<10
τ or t (s)	1.125–2	5–60	30–180
Q (mL min^{-1})	24–43	0.75–6	–

The Napierian molar absorption coefficient of the potassium ferrioxalate κ_λ was experimentally determined according to wavelengths using a spectrometer (Ultraspec 1000 Pharmacia Biotech®), as shown in Figure 3. It can be observed that κ_λ was relatively important from 300 nm and it progressively decreased from 300 nm to 490 nm. This means that, for a given concentration, the Napierian absorbance A_e (see next section) was strong around 300 nm, weak near 450 nm and zero above 490 nm. Consequently, the different wavelengths emitted by the mercury lamp were not equally absorbed, thus justifying the use of the polychromatic model.

In Figure 3, it is also interesting to note that the quantum yield of the ferrioxalate system varied little with the wavelength (data extracted from Hatchard and Parker (1956)): it remained ranged between 1 and 1.2.

2.4 Protocol for implementing the actinometry method

2.4.1 Potassium ferrioxalate preparation

In this study, potassium ferrioxalate was first prepared by mixing 3 volumes of potassium oxalate monohydrate $K_2C_2O_4\ H_2O$ [#CAS: 6487-48-5] (1.5 mol L^{-1}) and 1 volume

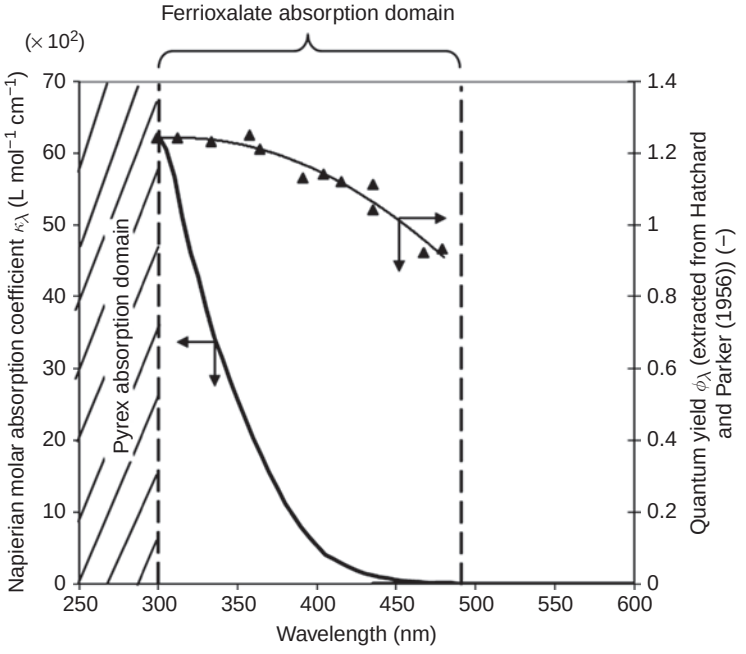

Figure 3 Dependence of the actinometer properties on the wavelength (Napierian molar absorption coefficient, quantum yield)

of ferric chloride $FeCl_3$ [#CAS: 7705-08-0] (1.5 mol L^{-1}). The potassium ferrioxalate precipitate was then filtered, recrystallized three times in water and dried at 40°C for 20 hours. Then, an appropriate mass of potassium ferrioxalate was dissolved in sulphuric acid solution to obtain a potassium ferrioxalate solution of $C_{A0} = 0.16$ mol L^{-1} (the concentrations in sulphuric acid are reported in Table 2). A second protocol was tested, which consisted of directly preparing the potassium ferrioxalate solution ($C_{A0} = 0.16$ mol L^{-1}) in sulphuric acid solution by adding the appropriate amount of potassium oxalate and ferric chloride. Various actinometry experiments were performed using either the first or the second protocol. No differences were observed in terms of conversion, thus demonstrating that the two protocols were equivalent.

Finally, note that the whole procedure (potassium ferrioxalate preparation and analysis) was carried out under red light to avoid potassium ferrioxalate decomposition.

2.4.2 Ferrioxalate analysis

Potassium ferrioxalate decomposition is commonly evaluated by complexation of the ferrous ions produced with o-phenanthroline, leading to a complex with a strong red colour. In our trials, for the photoreactors, 2 mL (V_0) of the samples was firstly diluted with 50 mL of deionized water ($V_1 = 52$ mL). Then 2 mL (V_2) of the diluted samples were mixed with 5 mL of o-phenanthroline ($C_{\text{o-phenanthroline}} = 1$ g L^{-1}), 5 mL of buffer solution (prepared with 36 mL of sulphuric acid 1 mol L^{-1}, 60 mL of sodium acetate 1 mol L^{-1} and completed to 100 mL with water) and finally 5 mL of water ($V_3 = 17$ mL). Samples were stirred for 30 min. The absorbance of the samples was recorded at 510 nm. Then, conversion was calculated as follows:

$$X = \frac{C_{Fe^{2+}}}{C_{A0}} = \frac{1}{C_{A0}} \frac{A_{510}}{k} \frac{V_3}{V_2} \frac{V_1}{V_0} \tag{7}$$

where A_{510} is the absorbance of the mixture, k is the slope of the calibration curve $A_{510} = f(C_{Fe^{2+}})$ obtained by using the standard solutions of Fe^{2+}/o-phenanthroline prepared according to the procedure described by Hatchard and Parker (1956). In the present study, the slope of the calibration curve k was found to be 10,980 L mol^{-1}.

3 Modelling

3.1 Case 1: monochromatic source

Potassium ferrioxalate, like many actinometers, can be described with the following reaction scheme:

$$A \xrightarrow{h\upsilon} B \tag{8}$$

If the batch photoreactor can be assumed to be perfectly mixed, the consumption rate of the compound A in the entire volume of the reactor can be expressed, for a monochromatic source of wavelength λ, as:

$$-\frac{dC_A}{dt} = \varphi_\lambda < L^a_{p,\lambda} > \tag{9}$$

where C_A is the mean concentration of the compound A in the reactor and φ_λ is the quantum yield of the reaction at the wavelength λ (mol einstein^{-1}).

$< L^a_{p,\lambda} >$ is the mean absorbed photon flux density by the compound A at the wavelength λ (expressed in einstein m^{-3} s^{-1}). This parameter is obtained by averaging, over the entire volume of the reactor (V_r), the absorbed local radiance $L^a_{p,\lambda}$ which, considering a collimated beam of radiation, is written as Cassano et al. (1995):

$$L^a_{p,\lambda} = \kappa_\lambda C_A L_{p,\lambda} \tag{10}$$

κ_λ is the Napierian molar absorption coefficient (m^2 mol^{-1}) of compound A at the wavelength λ and $L_{p,\lambda}$ is the photon radiance at the wavelength λ (einstein m^{-2} s^{-1}) which is determined from the radiative balance equation:

$$\nabla(L_{p,\lambda}\boldsymbol{u}) = -\kappa_\lambda C_A L_{p,\lambda} \tag{11}$$

where $\boldsymbol{u}$ is the directional unit vector of the light beam direction.

Eq. (11) requires the introduction of the incoming photon radiance $L^w_{p,\lambda}$ at the surface surrounding the absorbing volume, i.e. the incident photon radiance at the reactor wall. Note that, as we consider a collimated beam, this photon radiance $L^w_{p,\lambda}$ can also be called the flux density of photons received at the reactor wall.

Finally, considering a perfectly mixed batch photoreactor, a single absorbing species (compound A) at the wavelength of interest λ and a collimated beam of radiation with a direction $\boldsymbol{u}$ perpendicular to the irradiated surface, the absorbed photon flux density is expressed as follows:

$$< L^a_{p,\lambda} > = \frac{q_{p,\lambda}}{V_r} f_\lambda \tag{12}$$

where f_λ is the fraction of the light absorbed at the wavelength λ defined as:

$$f_\lambda = 1 - e^{-A_e} = 1 - e^{-\kappa_\lambda C_A l} \tag{13}$$

With A_e the Napierian absorbance and l the optical path length.

In eq. (12), $q_{p,\lambda}$ is the photon flux received (einstein s^{-1}) over the entire volume of reactor at the wavelength λ. It depends on the incoming photon flux at the surface

surrounding the absorbing volume ($q_{p0,\lambda}$) and on the reactor material transmittance (T_λ), such as:

$$q_{p,\lambda} = q_{p0,\lambda} T_\lambda \tag{14}$$

Note that, in this study, $q_{p,\lambda}$ and $q_{p0,\lambda}$ are equal. Indeed, we assume the photoreactor material (i.e. Pyrex or FEP) perfectly transparent to UV radiation above 300 nm.

The flux density of photons $L^w_{p,\lambda}$ received at the reactor wall (at the wavelength λ) can be calculated from the photon flux $q_{p,\lambda}$ (see Table 3) (Roger and Villermaux 1983). For that, a parallel plate reactor model with a thickness equal to the inner tube diameter ($l = d$) and illuminated from one side is considered for the two microphotoreactors, whereas a perfect annular geometry is assumed for the batch photoreactor (R_w is the inner radius of the immersion well and R_{w+l} is the outer radius, as illustrated in Figure 1c). Finally, note that this calculation assumes that the flux density of photons received on the reactor wall is homogeneous.

Table 3 Calculations of the flux density of photons $L^w_{p,\lambda}$

Photoreactors	l (m)	L^w_p (einstein m^{-2} s^{-1})
Continuous flow microphotoreactors	d	$\frac{q_p d}{V_r}$
Batch photoreactor	$R_{W+l} - R_w$	$\frac{q_p\left(R^2_{W+l} - R^2_W\right)}{2V_r R_w}$

A practical operating condition is to work under full absorption so as to use the incident light optimally (i.e. not to waste incident photons). This situation occurs when the fraction of light absorbed f_λ tends to 1. In this case, $q_{p,\lambda}$ is determined directly from the slope of the curve of the concentration of compound A versus time. Nevertheless, as the optical path length l is short in the microphotoreactors ($l = d = 508$ μm) and the actinometer solubility is low, full absorption conditions are difficult to obtain. Consequently, partial absorption conditions ($f_\lambda < 1$) classically occur in the microphotoreactors and thus, the exponential term in eq. (12) must be taken into account.

Finally, the use of eqs (9), (12), (13) and (14) leads to the following integrated equation:

$$\left(\varphi_\lambda \frac{q_{p,\lambda}}{V_r}\right) t = C_{A0} X + \frac{1}{\kappa_\lambda l} \ln\left[\frac{1 - e^{-\kappa_\lambda C_{A0} l}}{1 - e^{-\kappa_\lambda C_{A0}(1-X) l}}\right] \tag{15}$$

where X is the actinometer conversion defined as:

$$C_A = C_{A0}(1 - X) \tag{16}$$

We recall that eq. (15) is valid when the following conditions are fulfilled (Aillet et al. 2013; Shvydkiv et al. 2010): (i) a perfectly mixed batch photoreactor, (ii) a single absorbing species, (iii) a monochromatic light source, (iv) a collimated beam of radiation. The first two conditions are always satisfied when the actinometry method is implemented because the conversion is kept low (i.e. the distribution of the concentration remains close to the one initially assumed to be homogeneous and the main absorbing species is the initial reactant).

However, eq. (15) also remains true if, instead of a perfectly mixed batch photoreactor, we consider a continuous photoreactor that can be modelled as a plug flow reactor. In that case, the irradiation time t in eq. (15) should be replaced by the residence time τ defined as:

$$\tau = \frac{V_r}{Q} \tag{17}$$

We will later use eqs (15) and (17) to calculate the photon flux $q_{p,\lambda}$ received in the microphotoreactor B irradiated by the UV-LED array (at 365 nm).

3.2 Case 2: polychromatic source

In this study, the microphotoreactor A and the batch photoreactor were irradiated by the mercury vapour discharge lamp, which was polychromatic (Figure 2), and no radiation filters were used in our experiments. In such cases, eq. (15) is no longer valid. To overcome this limitation, a more complex model should be considered. It consists in discretizing the range of wavelengths covered by the lamp emission into several elementary intervals $\Delta\lambda_i$ in which the wavelength-dependent parameters (quantum yield φ_λ, material transmittance T_λ, and Napierian molar absorption coefficient κ_λ) can be averaged and considered constant (Zalazar et al. 2005). As the lamp has emitted line, each line corresponds to a wavelength interval $\Delta\lambda_i$.

Thus, an equation similar to eq. (9) exists for all discrete wavelength intervals $\Delta\lambda_i$ and can be written by introducing the density function g_λ of the lamp (eq. (5)) as:

$$\begin{aligned} \frac{dX}{dt} &= \frac{1}{C_{A0}} \frac{q_{p,0}}{V_r} \sum\nolimits_{\Delta\lambda i} \left[T_{\lambda_i} \varphi_{\lambda_i} g_{\lambda_i} f_{\lambda_i}\right] \\ &= \frac{1}{C_{A0}} \frac{q_{p,0}}{V_r} \sum\nolimits_{\Delta\lambda i} \left[T_{\lambda_i} \varphi_{\lambda_i} g_{\lambda_i} \left(1 - e^{-\kappa_{\lambda_i} C_{A0}(1-X) l}\right)\right] \end{aligned} \tag{18}$$

where q_{p0} is the *total* incoming photon flux at the surface surrounding the absorbing volume (the term "total"

meaning for all discrete wavelength intervals $\Delta\lambda_i$ emitted by the lamp).

Note that, in eq. (18), the term ($T_{\lambda_i}\,\varphi_{\lambda_i}\,g_{\lambda_i}\,f_{\lambda_i}$) is equal to zero:

- in the batch photoreactor and the microphotoreactor A, for each $\Delta\lambda_i$ below 300 nm as the Pyrex transmittance T_λ is considered equal to zero (eq. (1)),
- in the microphotoreactor B, for each $\Delta\lambda_i$ below 230 nm as the FEP transmittance T_λ is then considered equal to zero,
- whatever the photoreactors, for each $\Delta\lambda_i$ above 490 nm as the Napierian molar absorption coefficient of the actinometer κ_λ is considered equal to zero (Figure 3).

The next step is to solve eq. (18) numerically and to determine q_{p0} by minimizing the quadratic error R (Gauss–Newton algorithm) defined as:

$$R = \sum_i \left[(X)^i_{model} - (X)^i_{exp}\right]^2 \tag{19}$$

The photon flux received (einstein s^{-1}) over the entire volume of reactor at the wavelength λ, $q_{p,\lambda}$, is calculated from the material transmittance T_λ and the density function g_λ of the lamp, such as:

$$q_{p,\lambda} = T_\lambda\, g_\lambda\, q_{p0} \tag{20}$$

At last, the total photon flux received (einstein s^{-1}) over the entire volume of reactor, q_p, is deduced from:

$$q_p = \sum_{\Delta\lambda i} \left[q_{p,\lambda_i}\right] \tag{21}$$

As in case 1 (monochromatic source), q_p and q_{p0} are equal in this study ($T_{\lambda>300} = 1$ for Pyrex and $T_{\lambda>230} = 1$ for FEP).

Eq. (18) will thus be used for calculating the photon flux q_p received in the microphotoreactor A (in this case, t will be replaced by τ defined in eq. (17)) and in the batch photoreactor, both being irradiated by the mercury lamp.

4 Results

4.1 Microphotoreactor A

4.1.1 Photon flux received

Figure 4 presents the experimental conversions in potassium ferrioxalate versus irradiation times (i.e. residence times) in the microphotoreactor A irradiated by the polychromatic mercury lamp. Note that no experimental measurements were possible for residence times below 1.13 seconds because the pressure drop involved was too high. The experimental data reported, which correspond to several runs, are reproducible and show little dispersion (less than 10 %) despite the multiple dilutions associated with the analytical method. As already observed in the literature (Coyle and Oelgemöller 2008; Oelgemoeller 2012; Knowles, Elliott, and Booker-Milburn 2012; Mozharov et al. 2011; Aillet et al. 2013; Sugimoto et al. 2009; Shvydkiv et al. 2011; Aida et al. 2012), the times required to reach a given conversion are very short in comparison with those found in conventional photoreactors. This is mainly due to the fact that the number of reacting species moles involved ($C_{A0}\,V_r$) compared to the photon flux received is smaller in microphotoreactors, as we showed in a previous paper (Aillet et al. 2013).

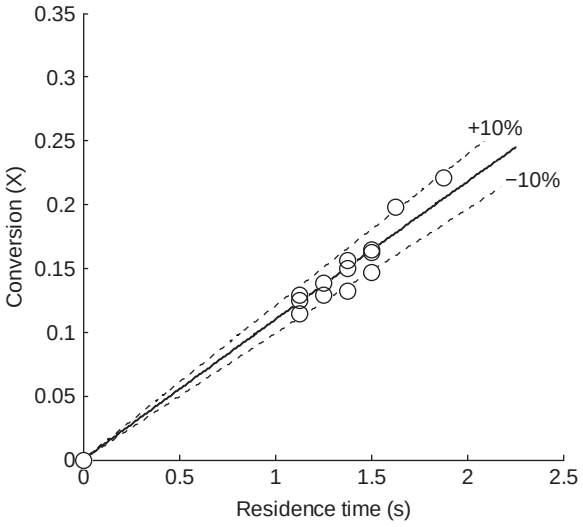

Figure 4 Actinometer conversion versus irradiation time in the microphotoreactor A. Experimental conversions (O) and conversions predicted by eq. (18) (–)

Figure 4 also shows good agreement between the conversions predicted by the polychromatic model (eq. (18)) and the experimental ones, thus confirming the relevancy of the assumptions made in the modelling.

From this modelling (eq. (18)), the photon flux q_p received in the microphotoreactor was found to be equal to:

$$q_p = 26.2 \times 10^{-6}\ \text{einstein}\,s^{-1} \tag{22}$$

4.1.2 Polychromatic source model versus monochromatic source model

From the received photon flux q_p calculated above (eq. (22)), it is interesting to look for the photon flux $q_{p,\lambda}$ received at

Table 4 Photon flux ($q_{p,\lambda}$) received at each wavelength in the microphotoreactor A

λ (nm)	$q_{p,\lambda}$ (10^{-6} einstein s^{-1})	λ (nm)	$q_{p,\lambda}$ (10^{-6} einstein s^{-1})
254	0.44	365	4.07
265	0.85	405	1.32
280	0.43	436	3.69
297	0.51	546	6.34
302	1.24	577	2.41
313	2.05	579	2.37
334	0.48		

each wavelength λ emitted by the mercury lamp. For this purpose, the density function of the lamp g_λ and the material transmittance T_λ should be introduced as shown in eq. (20).

Table 4 shows the associated values at each wavelength. Given the lamp density function, it is logically observed that the main photon fluxes received correspond to 365 nm, 436 nm and 546 nm. However, it can be seen that, despite the fact that the actinometer absorbs only in the range between 300 nm and 490 nm, this modelling makes it possible to determine the photon flux received at other wavelengths. The photon fluxes received for wavelengths below 300 nm are reported in Table 4 but we should keep in mind that these values will never be received in the photoreactor, unless the vessel material is changed for a transparent material such as quartz. Concerning the photon fluxes received for wavelengths above 490 nm, the accuracy of the values reported strongly depends on the validity of the assumption made on the material transmittance ($T_{\lambda>490} = 1$).

It is interesting to discuss the consequences on a common hypothesis that would assimilate the mercury lamp to a monochromatic source. In this framework, it is logical, considering the absorption domain of the ferrioxalate actinometer (Figure 3) and the emission spectrum of the lamp (Figure 2), to choose 365 nm as the main wavelength taking part in the photoreaction. The photon flux received q_p is then calculated from eqs (15) and (17) by taking the quantum yield and the Napierian molar absorption coefficient at the wavelength of 365 nm. The following value is obtained:

$$q_p = 11.2 \times 10^{-6} \text{ einstein s}^{-1} \quad (23)$$

When this is compared to the photon flux calculated by eq. (22) (i.e. polychromatic model), significant differences are observed. Such findings are not surprising:

- Firstly, the photon flux obtained in eq. (23) does not represent the real flux at 365 nm but is the result of the contributions of all the wavelengths, which are assumed to be absorbed equally to the wavelength of 365 nm (i.e. the Napierian molar absorption coefficient and the quantum yield at 365 nm are considered).
- Secondly, this photon flux of 11.2×10^{-6} einstein s^{-1} does not take account of the lamp wavelengths that are not absorbed. This can have important consequences. For example, consider a photochemical synthesis carried out in the microphotoreactor A for which the absorption domain of the absorbing species differs from that of the actinometer species. In this case, this photon flux will not be valid. In an extreme case, let us imagine that, for this photochemical reaction, the species absorbs weakly around 365 nm but strongly at 546 nm. It is clear that this photon flux calculated at 365 nm by considering a monochromatic source will no longer be valid, as the potassium ferrioxalate actinometer does not absorb at 546 nm.

For these reasons, it is strongly recommended to use the polychromatic modelling (eq. (18)) to calculate the photon flux received q_p in a photoreactor irradiated with polychromatic light when no light filtering is used. For the continuous flow microphotoreactor A, the received photon flux given by eq. (22) should thus be considered instead of the one given by eq. (23).

4.2 Microphotoreactor B

Figure 5a presents the conversions in potassium ferrioxalate versus irradiation times (i.e. residence times) in the microphotoreactor B when the UV-LED array is supplied with different current intensities (ranging from 100 mA to 400 mA). Good agreement is also observed here between the conversions predicted by the monochromatic model (eqs (15) and (17)) and the experimental conversions.

In Figure 5b, the photon flux received in the reactor at $\lambda = 365$ nm is plotted as a function of the current intensity supplying the UV-LED array. The curve $q_p = f(I_a)$ is linear with a correlation coefficient > 0.99, which is in agreement with the LED manufacturer's data.

Finally, the maximum current intensity recommended by the LED manufacturer being 500 mA, the maximum photon flux that can be received in the microphotoreactor B can be extrapolated from Figure 5b:

$$q_p = 3.82 \times 10^{-7} \text{ einstein s}^{-1} \quad (24)$$

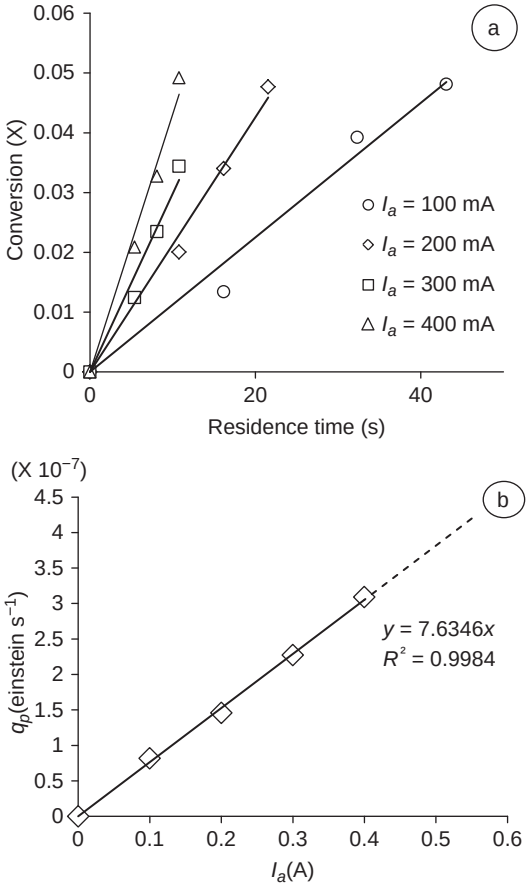

Figure 5 (a) Actinometer conversion versus irradiation time in the microphotoreactor B for different current intensities supplying the UV-LED array. Experimental conversions (symbols) and conversions predicted by eqs (15)–(17) (straight lines). (b) Photon flux received versus the current intensity supplying to the UV-LED array

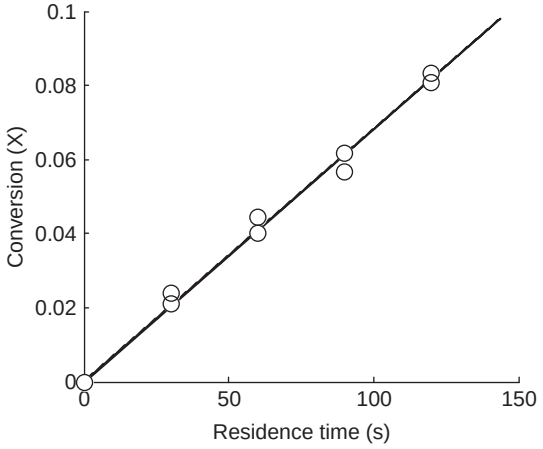

Figure 6 Actinometer conversion versus irradiation time in the batch photoreactor. Experimental conversions (O) and conversions predicted by eq. (18) (–)

Table 5 Photon flux ($q_{p,\lambda}$) received in the batch photoreactor at each wavelength emitted by the mercury lamp

λ (nm)	$q_{p,\lambda}$ (10^{-6} einstein s^{-1})	λ (nm)	$q_{p,\lambda}$ (10^{-6} einstein s^{-1})
254	0.79	365	7.40
265	1.55	405	2.39
280	0.78	436	6.70
297	0.93	546	11.53
302	2.24	577	4.38
313	3.72	579	4.30
334	0.87		

4.3 Batch photoreactor

Figure 6 presents the experimental conversions in potassium ferrioxalate versus irradiation times in the batch photoreactor irradiated by the polychromatic mercury lamp. It can be observed that the irradiation times required to reach a given conversion are significantly higher than in the continuous microphotoreactors. As shown by Aillet et al. (2013), this is linked with the fact that the number of reacting species moles involved ($C_{A0}\,V_r$) compared to the photon flux received is larger in the batch photoreactor.

Using the same methodology as for the microphotoreactor A (i.e. the polychromatic model described by eq. (18)), the photon flux received in the batch photoreactor irradiated by the mercury lamp was calculated:

$$q_p = 47.6 \times 10^{-6}\text{einstein s}^{-1} \tag{25}$$

Again, we can express the above value for eachwavelength emitted by the mercury lamp with the help of the emission density function of the lamp (eq. (20)). The same conclusions can be drawn as from Table 5.

5 Discussion

5.1 Comparison between the power received in the photoreactors and the radiant power emitted by the lamp

The photon fluxes received in each photoreactor (eqs (22), (24) and (25)) can be also expressed in radiometric units (i.e. in watts) according to:

$$q_{e,\lambda} = q_{p,\lambda}\,\Delta E_\lambda\,N_A \tag{26}$$

In the case of a polychromatic source (batch photoreactor and microphotoreactor A), the total radiant power is then

obtained by summing the radiant power emitted at each wavelength:

$$q_e = \sum\nolimits_{\Delta\lambda_i} q_{e,\lambda_i} \quad (27)$$

In eq. (27), the photon fluxes at wavelengths below 300 nm are not taken into account as the Pyrex transmittance is considered equal to zero.

These values are reported in Table 6, together with the lamp radiant power P given by the manufacturer, for comparison purposes. Clearly, whatever the photoreactor, the power actually received inside it is less than 11% of the lamp radiant power.

Table 6 Total photon flux received (q_e) and lamp radiant power (P) for each photoreactor

Parameters	Microphotoreactor		Batch photoreactor
	A	B	
Lamp radiant power (manufacturer's data) P (W)	125	2.925	125
Power received q_e (W)	6.07	0.13	11.9

In the case of the mercury lamp, this difference can be explained by the fact that the majority of the emission is in the infrared domain (that is why a cooling system should be used in such systems).

With the UV-LED array, this value is low in comparison with the total radiant power emitted of 2.925 W, meaning that the design of the microphotoreactor B is not optimal. In the future, it could be easily improved by increasing the tube length under the area irradiated by the UV-LED array, or by adding some reflectors.

Finally, these findings demonstrate that the photon flux actually received in the reactor must imperatively be measured as it can be very different from a rough estimation based on the power emitted from the lamp, which does not take the reactor exposition, or the reflectance and transmittance of the reactor material into account. Such measurements would also be a useful tool for optimizing the photoreactor design and exposition with respect to the light source.

5.2 Comparison of photoreactors

The objective of this last section is to compare the different photoreactors investigated in this study by using the measured photon fluxes received. To do this, we consider the wavelength of 365 nm. In consequence, for the two photoreactors irradiated with the polychromatic mercury lamp, the values in Table 7 are calculated from the lamp density function at this wavelength of 365 nm. Rigorously speaking, the following comparison is valid only for plug flow reactors or perfectly mixed photoreactors, that is to say when the mixing phenomena along the optical path length, i.e. in each cross-sectional area of the reactor (plug-flow reactor), or in the entire volume of the reactor (perfectly mixed photoreactor) are strong enough to ensure homogeneous concentration. Lastly, this comparison will assume that the fraction of light absorbed f_λ is identical in the three photoreactors.

Table 7 Photon flux (q_p) received, absorbed photon flux density ($\frac{q_p}{V_r}$) and photon flux density received at the reactor wall (L_p^w) at a wavelength of 365 nm in the different photoreactors

Parameters	Microphotoreactor		Batch photoreactor[a]
	A[a]	B	
q_p (10^{-6} einstein s^{-1})	4.07	0.382	7.40
$\frac{q_p}{V_r}$ (einstein m^{-3} s^{-1})	5.02	0.71	0.033
L_p^w (10^{-3} einstein m^{-2} s^{-1})	2.55[b]	0.36[b]	0.17[c]

Notes: [a] The values correspond to the wavelength of 365 nm when the light source is the polychromatic mercury lamp; [b] L_p^w is calculated by assuming that the microphotoreactors can be described as parallel plate reactors ($l = d$) (see Table 3); [c] L_p^w is calculated by using annular geometry to describe the batch photoreactor (see Table 3).

From the photon flux received q_p at 365 nm for each photoreactor, the absorbed photon flux density $\frac{q_p}{V_r}$ and the photon flux density received L_p^w at the reactor wall (Table 3) can be calculated: they are reported in Table 7. The comparison of the photoreactors depends on the criteria that we choose to evaluate their performances.

If the productivity (moles of compound produced per time unit) is selected as the main criterion, it is interesting to look at the photon flux received q_p because it is directly correlated with the productivity. Considering the small amount $\mathrm{d}N = V_r\, C_{A0}\, \mathrm{d}X$ generated in the small irradiation time interval $\mathrm{d}t$, the productivity can be related to the photon flux q_p as follows:

$$\text{Productivity} = \frac{\mathrm{d}N}{\mathrm{d}t} = q_{p,0} \sum\nolimits_{\Delta\lambda_i} \left(T_{\lambda_i}\, \varphi_{\lambda_i}\, g_{\lambda_i}\, f_{\lambda_i}\right) = \mathrm{F}_1\left(q_p\right) \quad (28)$$

In this case, it can be observed that the batch photoreactor was more efficient in this study (Table 7). Nevertheless, the microphotoreactor A could easily be improved by increasing the tube length so as to receive more light. In the case of the microphotoreactor B, the radiant power of the

UV-LED array is still lower than that of the classic mercury lamp, even though some promising improvements in LED powers can be expected in the future. Moreover, from Table 6, it is clear that the design of the microphotoreactor B can be optimized (for example by increasing the tube length) since only 4.5% of the radiant lamp power is received.

The performance of each photoreactor can also be assessed using the differential Space Time Yield (*STY*). This parameter evaluates the small amount $\mathrm{d}N = V_r\, C_{A0}\, \mathrm{d}X$ generated in the time interval $\mathrm{d}t$ and per unit of volume V_r is directly related to the photon flux received per unit volume, $\frac{q_p}{V_r}$ as:

$$\mathrm{STY} = \frac{1}{V_r}\frac{\mathrm{d}N}{\mathrm{d}t} = \mathrm{F}_2\left(\frac{q_p}{V_r}\right) \tag{29}$$

Based on this criterion, the two microphotoreactors are clearly the most efficient (eq. (30)), as commonly observed in previous studies (Aillet et al. 2013; Sugimoto et al. 2009; Shvydkiv et al. 2011; Aida et al. 2012; Shvydkiv et al. 2010):

$$\begin{cases} \dfrac{\mathrm{STY}_A}{\mathrm{STY}_{batch}} = \dfrac{\left(\frac{q_p}{V_r}\right)_A}{\left(\frac{q_p}{V_r}\right)_{batch}} = 153 \\ \dfrac{\mathrm{STY}_B}{\mathrm{STY}_{batch}} = \dfrac{\left(\frac{q_p}{V_r}\right)_B}{\left(\frac{q_p}{V_r}\right)_{batch}} = 22 \end{cases} \tag{30}$$

This parameter has made the success of microreactors as such systems enable small amounts of products to be obtained quickly, which is an undeniable advantage in the R&D field as it improves the screening of new reaction pathways.

Finally, we can look at the photon flux density received at the irradiated wall L_p^w (Table 7) in order to compare photoreactors. In this case, it is interesting to note that the microphotoreactor B and the batch photoreactor are quite similar, whereas the microphotoreactor A exhibits a higher L_p^w. A direct comparison of the photoreactors based on this parameter is still difficult. Nevertheless, it must be kept in mind that too high a value of the photon flux density at the reactor wall L_p^w can be a drawback, in particular when the reagents are likely to decompose under excessive light or when there are several absorbing species in the medium. The mixing along the light path length inside the reactor could be insufficiently efficient to renew the area close to the irradiated surface and would thus cause excessive light exposure of the absorbing species present. The potential consequences are a photodegradation of the products and/or a drastic decrease in the reaction rate since the exchange of reactants out of and into the area close to the irradiated surface would be limited. In these circumstances, the reactor comparison proposed above is no longer valid and more advanced modelling becomes necessary to accurately predict reaction conversion and selectivity. Such advanced modelling is based on the resolution, in two or three spatial dimensions, of the radiative transfer equation (eq. (11)) coupled with fundamental conservation equations (mass, momentum and energy). The photon flux density received at the reactor wall L_p^w that is here measured then becomes essential data as it constitutes one of the boundary conditions of the system of equations to be solved.

6 Conclusions

The photon fluxes received in two continuous flow microphotoreactors were measured accurately and easily by actinometry. Whatever the photoreactor, significant differences between the photon flux actually received and the radiant power emitted by the lamp were highlighted, thus confirming the importance of such in situ measurements. Some guidelines based on a knowledge of the photon flux were also proposed to compare various photoreactors. In future studies, this photon flux will constitute a key data for sizing a microphotoreactor according to the photochemical reaction under test and/or for transposing a photochemical reaction from a conventional batch reactor to an intensified continuous flow reactor.

References

Aida, Shin, Kimitada Terao, Yasuhiro Nishiyama, Kiyomi Kakiuchi, and Michael Oelgemöller. 2012. "Microflow Photochemistry – A Reactor Comparison Study Using the Photochemical Synthesis of Terebic Acid as a Model Reaction." *Tetrahedron Letters* 53:5578–81.

Aillet, Tristan, Karine Loubiere, Odile Dechy-Cabaret, and Laurent Prat. 2013. "Photochemical Synthesis of a 'Cage' Compound in a Microreactor: Rigorous Comparison with a Batch Photoreactor." *Chemical Engineering and Processing: Process Intensification* 64:38–47.

Allmand, Arthur John, and Kenneth William Young. 1931. "CCCCXXIV. The Photolysis of Potassium Ferrioxalate Solutions. Part III." *Journal of the Chemical Society* 3079–87.

Cassano, Alberto E., Carlos A. Martin, Rodolfo J. Brandi, and Orlando M. Alfano. 1995. "Photoreactor Analysis and Design: Fundamentals and Applications." *Industrial & Engineering Chemistry Research* 34:2155–201.

Cornet, Jean-François, Anne Marty, and Jean-Bernard Gros. 1997. "Revised Technique for the Determination of Mean Incident Light Fluxes on Photobioreactors." *Biotechnology Progress* 13 (4):408–15.

Coyle, Emma E., and Michael Oelgemöller. 2008. "Micro-Photochemistry: Photochemistry in Microstructured Reactors. The New Photochemistry of the Future?" *Photochemical & Photobiological Sciences* 7:1313–22.

Hatchard, C. G., and C. A. Parker. 1956. "A New Sensitive Chemical Actinometer. II. Potassium Ferrioxalate as a Standard Chemical." *Proceedings of the Royal Society of London Series A, Mathematical and Physical Sciences* 235:518–36.

Hook, Benjamin D. A., Wolfgang Dohle, Paul R. Hirst, Mark Pickworth, Malcolm B. Berry, and Kevin I. Booker-Milburn. 2005. "A Practical Flow Reactor for Continuous Organic Photochemistry." *The Journal of Organic Chemistry* 70:7558–64.

Knowles, Jonathan P., Luke D. Elliott, and Kevin I. Booker-Milburn. 2012. "Flow Photochemistry: Old Light through New Windows." *Beilstein Journal of Organic Chemistry* 8:2025–52.

Kuhn, H. J., S. E. Braslavsky, and R. Schmidt. 2004. "Chemical Actinometry (IUPAC Technical Report)." *Pure and Applied Chemistry* 76:2105–46.

Lainchbury, Michael D., Marcus I. Medley, Piers M. Taylor, Paul Hirst, Wolfgang Dohle, and Kevin I. Booker-Milburn. 2008. "A Protecting Group Free Synthesis of (±)-Neostenine via the [5 + 2] Photocycloaddition of Maleimides." *The Journal of Organic Chemistry* 73:6497–505.

Lehóczki, Tímea, Éva Józsa, and Katalin Ősz. 2013. "Ferrioxalate Actinometry with Online Spectrophotometric Detection." *Journal of Photochemistry and Photobiology A: Chemistry* 251:63–8.

Mozharov, Sergey, Alison Nordon, David Littlejohn, Charlotte Wiles, Paul Watts, Paul Dallin, and John M. Girkin. 2011. "Improved Method for Kinetic Studies in Microreactors Using Flow Manipulation and Noninvasive Raman Spectrometry." *Journal of the American Chemical Society* 133:3601–8.

Oelgemoeller, Michael. 2012. "Highlights of Photochemical Reactions in Microflow Reactors." *Chemical Engineering and Technology* 35:1144–52.

Parker, C. A. 1953. "A New Sensitive Chemical Actinometer. I. Some Trials with Potassium Ferrioxalate." *Proceedings of the Royal Society of London Series A, Mathematical and Physical Sciences* 220:104–16.

Roger, Maurice, and Jacques Villermaux. 1983. "Modelling of Light Absorption in Photoreactors Part II. Intensity Profile and Efficiency of Light Absorption in a Cylindrical Reactor Experimental Comparison of Five Models." *The Chemical Engineering Journal* 26:85–93.

Shvydkiv, Oksana, Sonia Gallagher, Kieran Nolan, and Michael Oelgemöller. 2010. "From Conventional to Microphotochemistry: Photodecarboxylation Reactions Involving Phthalimides." *Organic Letters* 12:5170–73.

Shvydkiv, Oksana, Alexander Yavorskyy, Su Bee Tan, Kieran Nolan, Norbert Hoffmann, Ali Youssef, and Michael Oelgemöller. 2011. "Microphotochemistry: A Reactor Comparison Study Using the Photosensitized Addition of Isopropanol to Furanones as a Model Reaction." *Photochemical & Photobiological Sciences* 10:1399.

Sugimoto, Atsushi, Takahide Fukuyama, Yukihito Sumino, Makoto Takagi, and Ilhyong Ryu. 2009. "Microflow Photo-Radical Reaction Using a Compact Light Source: Application to the Barton Reaction Leading to a Key Intermediate for Myriceric Acid A." *Tetrahedron* 65:1593–98.

Vaske, Yvette S. Mimieux, Maximillian E. Mahoney, Joseph P. Konopelski, David L. Rogow, and William J. McDonald. 2010. "Enantiomerically Pure Trans-β-Lactams from α-Amino Acids via Compact Fluorescent Light (CFL) Continuous-Flow Photolysis." *Journal of the American Chemical Society* 132:11379–85.

Yang, Quan, Pei Ling Ang, Madhumita B. Ray, and Simo O. Pehkonen. 2005. "Light Distribution Field in Catalyst Suspensions within an Annular Photoreactor." *Chemical Engineering Science* 60(19):5255–68.

Yang, Min K., Roger H. French, and Edward W. Tokarsky. 2008. "Optical Properties of Teflon® AF Amorphous Fluoropolymers." *Journal of Micro/Nanolithography, MEMS and MOEMS* 7:33010–330101.

Yang, Quan, Simo O. Pehkonen, and Madhumita B. Ray. 2004. "Evaluation of Three Different Lamp Emission Models Using Novel Application of Potassium Ferrioxalate Actinometry." *Industrial Engineering Chemistry Research* 43(4):948–55.

Zalazar, Cristina S., Marisol D. Labas, Carlos A. Martin, Rodolfo J. Brandi, Orlando M. Alfano, and Alberto E. Cassano. 2005. "The Extended Use of Actinometry in the Interpretation of Photochemical Reaction Engineering Data." *Chemical Engineering Journal* 109(1–3):67–81.